

Observations and model calculations of trace gas scavenging in a dense Saharan dust plume during MINATROC

M. de Reus¹, H. Fischer¹, R. Sander¹, V. Gros^{1,3}, R. Kormann¹, G. Salisbury¹, R. Van Dingenen², J. Williams¹, M. Zöllner¹, and J. Lelieveld¹

¹Max Planck Institute for Chemistry, PO Box 3060, 55020 Mainz, Germany

²Joint Research Centre, Ispra, Italy

³now at: Laboratoire des Sciences du Climat et de l'Environnement (LSCE), Gif sur Yvette, France

Received: 13 January 2005 – Published in Atmos. Chem. Phys. Discuss.: 11 February 2005

Revised: 2 May 2005 – Accepted: 13 June 2005 – Published: 20 July 2005

Abstract. An intensive field measurement campaign was performed in July/August 2002 at the Global Atmospheric Watch station Izaña on Tenerife to study the interaction of mineral dust aerosol and tropospheric chemistry (MINATROC). A dense Saharan dust plume, with aerosol masses exceeding $500 \mu\text{g m}^{-3}$, persisted for three days. During this dust event strongly reduced mixing ratios of RO_x (HO_2 , CH_3O_2 and higher organic peroxy radicals), H_2O_2 , NO_x (NO and NO_2) and O_3 were observed. A chemistry boxmodel, constrained by the measurements, has been used to study gas phase and heterogeneous chemistry. It appeared to be difficult to reproduce the observed HCHO mixing ratios with the model, possibly related to the representation of precursor gas concentrations or the absence of dry deposition. The model calculations indicate that the reduced H_2O_2 mixing ratios in the dust plume can be explained by including the heterogeneous removal reaction of HO_2 with an uptake coefficient of 0.2, or by assuming heterogeneous removal of H_2O_2 with an accommodation coefficient of 5×10^{-4} . However, these heterogeneous reactions cannot explain the low RO_x mixing ratios observed during the dust event. Whereas a mean daytime net ozone production rate (NOP) of $1.06 \text{ ppb}_v/\text{hr}$ occurred throughout the campaign, the reduced RO_x and NO_x mixing ratios in the Saharan dust plume contributed to a reduced NOP of $0.14\text{--}0.33 \text{ ppb}_v/\text{hr}$, which likely explains the relatively low ozone mixing ratios observed during this event.

1 Introduction

The interaction between atmospheric aerosols and photochemistry via heterogeneous reactions has been subject to intense investigation during the last decades. As an example, heterogeneous reactions on polar stratospheric clouds lead to the destruction of stratospheric ozone (e.g. Crutzen and Arnold, 1986). Heterogeneous reactions on cloud droplets and aerosols are also found to be important for tropospheric chemistry (e.g. Lelieveld and Crutzen, 1990). Special emphasis has been given to reactions on mineral dust aerosol (e.g. Usher et al., 2003), since these particles provide a large surface area for heterogeneous reactions in the troposphere (IPCC, 1996).

During several field campaigns a correlation between high dust loadings and low O_3 and HNO_3 concentrations has been observed (e.g. de Reus et al., 2000; Hanke et al., 2003; Bonasoni et al., 2004). The latter authors also showed that dust-poor airmasses originating in North Africa had significantly higher O_3 concentrations than those which carried dust.

Chemical boxmodels as well as global and regional chemical-transport models have been used to calculate the reduction in trace gas mixing ratios due to heterogeneous reactions on mineral dust aerosol. Most studies focussed on ozone and nitrogen species, while only a few studies report effects of mineral dust on OH and HO_2 mixing ratios. Zhang et al. (1994) and Zhang and Carmichael (1999), for example, used a boxmodel to simulate the loss of SO_2 , NO_x , HO_2 and O_3 due to heterogeneous reactions on mineral dust aerosol. Dentener et al. (1996) performed simulations with a global chemistry-transport model and calculated an O_3 reduction up to 10% in and nearby dust source areas. De Reus et al. (2000) calculated a 30–40% reduction of O_3 in a Saharan dust plume near the coast of Africa, attributed to the direct removal of O_3 by dust aerosol and the heterogeneous removal of HNO_3 .

Correspondence to: M. de Reus
(reus@mpch-mainz.mpg.de)

Bauer et al. (2004) calculated a 5% reduction in global tropospheric ozone and concluded that this was mainly due to the uptake of HNO_3 on dust aerosol and not due to the direct uptake of O_3 . However, the HNO_3 concentration was overestimated by the global model, which may have strongly biased the results of this study. Bian and Zender (2003) investigated the effect of reduced photolysis rates and heterogeneous chemistry on the tropospheric trace gas mixing ratios. They concluded that both processes cause a combined decrease in global mean O_3 of 0.7%, and 11.1% for OH, 5.2% for HO_2 and 3.5% for HNO_3 . The effects of heterogeneous removal reactions clearly dominated over the reduced photolysis rates. Tang et al. (2004) performed a model study using a regional-scale chemistry-transport model and compared the results with aerosol chemical composition measurements in a dust plume encountered during the ACE-Asia measurement campaign. They investigated both the reduction in solar (actinic) radiation and heterogeneous reactions on the dust aerosol. Low O_3 concentrations in the dust plume could only be explained by heterogeneous reactions. It was inferred that the reduction of photolysis rates largely determines changes in OH concentrations, whereas the large decrease in HNO_3 (up to 95%) and SO_2 (up to 55%) concentrations was due to heterogeneous reactions.

Although all aforementioned studies indicate a strong influence of mineral dust aerosols on tropospheric chemistry, the results are very different. This is mainly due to the large uncertainty in the uptake coefficients for the different trace gases on mineral dust aerosols. Moreover, for boxmodel calculations it has proven difficult to provide realistic initial conditions, and for all models the comparison with observations is a main challenge.

In this study we use an alternative approach. We employ a chemical boxmodel to analyse measurements performed within a dense Saharan dust plume at the Izaña observatory on Tenerife, Canary Islands. We use the model to calculate the steady state concentrations of RO_x , H_2O_2 and HCHO and compare them with observed values. For the model initialisation measured quantities are used to the extent possible. In addition to heterogeneous O_3 and HNO_3 uptake and the reduction of photolysis rates by mineral dust aerosol, as addressed in previous studies, we focus on the effects of HO_2 and H_2O_2 uptake in this study. Furthermore, we compare the net ozone production rate in the Saharan dust plume with airmasses not containing dust.

2 The MINATROC experiment

The MINATROC (MINeral dust And TROpospheric Chemistry) project was designed to investigate the effects of heterogeneous reactions involving mineral aerosol on tropospheric chemistry. The project combined three types of research activities: laboratory experiments to quantify selected interactions between trace gases and mineral dust aerosol,

field experiments to study the influence of mineral dust on tropospheric chemistry under realistic conditions, and global model studies to put the results of the former two into perspective. In this paper we will present observations of the second field experiment, performed in July/August 2002 at the Izaña observatory on the island of Tenerife, Spain.

Izaña observatory is part of the World Meteorological Organisation (WMO) Global Atmospheric Watch (GAW) network, and is operated by the Spanish Meteorological Institute. The station is situated on a mountain ridge on the island of Tenerife at 2360 m above sea level (a.s.l., $28^\circ 18' \text{N}$, $16^\circ 29' \text{W}$). Between 15 July and 15 August 2002 intensive aerosol and trace gas measurements were performed. The influence of mineral dust on the chemistry of the troposphere could be studied extensively during this period, since, besides several smaller dust episodes, a major dust event was probed between 28 and 31 July 2002.

3 Instrumentation

Additional to the set of measurements of the global watch program at Izaña, intensive measurements of aerosols and trace gases were performed during MINATROC by different institutes.

The instruments to measure atmospheric trace gases were operated by the Max Planck Institute for Chemistry, Mainz, Germany, from two laboratory containers. A sample air inlet was placed at the roof of both containers about 4 m above the ground. The RO_x instrument and the upward looking JNO_2 and JO^1D filter radiometers were deployed directly on the roof of the container at about 3 m above ground level, while the downward looking JNO_2 and JO^1D filter radiometers were mounted at a height of 1.5 m above ground level.

Table 1 lists the trace gas instruments which are relevant for this study, together with their associated uncertainties and detection limits. Since most instruments are similar to the ones which have been used during the first MINATROC field experiment at Mt. Cimone in June 2000, a detailed description of the O_3 , CO, RO_x , NO and NO_y instruments can be found in Fischer et al. (2003). For the other instruments more details are given below.

A liquid chemistry fluorescence detector (AERO laser model AL 4021) was used to measure formaldehyde (HCHO). The instrument first strips the HCHO from the ambient air into a strongly diluted H_2SO_4 solution, after which it reacts with acetylacetone and ammoniumacetate to form 3,5-diacetyl-1,4-dihydrolutidine (DDL) following the Hantzsch reaction. The fluorescence signal of the excited reaction product is detected by a photomultiplier at 510 nm. The same instrument has been employed during a previous aircraft campaign (Kormann et al., 2003).

For the determination of H_2O_2 a second liquid chemistry fluorescence detector has been used (AERO laser model AL 2001CA). After stripping H_2O_2 from the ambient air in a

Table 1. Instrumentation used for trace gas measurements during MINATROC.

Species	Measurement principle	Instrument	Uncertainty	Detection limit
O ₃	UV absorption	Ansyco 41M	<5%	1 ppbv
CO	Gas chromatograph	Thermo-Electron	5%	
NO	chemiluminescence detector (CLD)	ECOPHYSICS CLD 790SR	3%	8 ppt _v
NO ₂	CLD and photolytic converter (PLC)	ECOPHYSICS CLD 790SR and PLC 760	8% at night, 20% during the day	24 ppt _v
NO _y	CLD and catalytic converter	ECOPHYSICS CLD 770AL	5.6%	100 ppt _v
HCHO	Fluorescence detector (Hantzsch reaction)	Aero Laser AL4021	5%	23 ppt _v
H ₂ O ₂	Fluorescence detector (dual enzyme technique)	Aero Laser AL2001CA	20%	60 ppt _v
CH ₃ OOH	Fluorescence detector	AL2001CA	100% ¹	60 ppt _v
RO _x	Chemical amplifier and photoluminescence detector	PERCA and Luminox LMA-3	30–40%	2 ppt _v
Acetone, methanol, isoprene	Proton-Transfer-Reaction Mass Spectrometer (PTRMS)		<28%	55 ppt _v , 213 ppt _v , 46 ppt _v
Propane, butane	Gas chromatograph-mass spectrometer (GC-MS)	Agilent GC-MS 6890/5973	<15%	3 ppt _v
JO ¹ D	Filter Radiometer	METCON	20% ² –30% ³	8 × 10 ⁻⁷ s ⁻¹
JNO ₂	Filter Radiometer	METCON	10% ² –20% ³	8 × 10 ⁻⁷ s ⁻¹

¹ Estimated uncertainty for the CH₃OOH measurements, see text.

² For solar zenith angles <60°

³ For solar zenith angles between 60° and 70°

slightly acidic solution, this instrument determines the total peroxide concentration by the liquid phase reaction of peroxides with p-hydroxyphenylacetic acid, catalysed by peroxidase. To distinguish between H₂O₂ and organic peroxides two parallel channels are used. In one channel H₂O₂ is selectively destroyed by the enzyme catalase prior to the fluorescence detection in the instrument. The difference between the signals from both channels is a measure for the H₂O₂ concentration (Lazrus et al., 1986).

No quantification of organic peroxides can be achieved without knowing the specific peroxide composition in the atmosphere. This is due to the high variability in the relative amounts of peroxides in ambient air, the large variations in Henry's law constants, and, consequently, the collection efficiencies for these compounds. However, if we assume that the most abundant organic peroxide in the atmosphere is methylhydroperoxide (MHP, CH₃OOH) and that the collection efficiency of MHP is 60%, an upper limit for the MHP mixing ratio can be determined. The obtained CH₃OOH mixing ratio should, however, be interpreted with considerable care.

The calibration of both AERO laser detectors was carried out both in the gas and the liquid phase. HCHO calibration gas was produced using a VICI Metronics permeation tube operated at a temperature of 80°C, while for H₂O₂ a home-built permeation device was used, consisting of a semi-

permeable polyethylene tube which was placed in a saturated H₂O₂ environment (glass bottle with a small amount of 30% H₂O₂ solution, operated at a constant temperature of 30°C). Zero air (CAP60 Headline Filters air purifier) with a total flow of 6L/min was mixed with the calibration gas stream leading to a mixing ratio of 13.3 ppbv HCHO and 5.9 ppbv H₂O₂. Every 4–6 h calibration gas was added to the sample air at the top of the sample mast, to determine the losses of HCHO and H₂O₂ in the inlet line. To test the stability of the instrument, additional liquid calibrations were performed once a day with 1 μM HCHO and H₂O₂ solutions. Laboratory calibrations show that 7.4% ± 2.7% of the H₂O₂ is lost in the inlet line, while no reduction of the HCHO mixing ratio was observed due to the long inlet line.

Measurements of a range of volatile organic carbons (VOC) were performed using a proton-transfer-reaction mass spectrometer (PTRMS). Inside this instrument organic species are chemically ionised by the proton transfer with H₃O⁺ ions and the products are detected with a quadrupole mass spectrometer (Lindinger et al., 1998). In this study the measurements of acetone, methanol and isoprene are used. The isoprene mixing ratios measured with the PTRMS, however, should be regarded as upper limits, due to other possible contributions to this mass (Williams et al., 2001). More details about the measurement technique and calibration procedure can be found in Salisbury et al. (2003).

For the measurement of non methane hydrocarbons (NMHC) stainless steel canister samples were taken every 3 or 6 h during the campaign, which were analysed in the laboratory of the Max Planck Institute in Mainz, using a gas chromatograph-mass spectrometer system (GC-MS). Due to the set-up of the GC-MS system only hydrocarbons with more than 2 C atoms were analysed. More details about the collection of the samples, the GC-MS system and its calibration procedure can be found in Gros et al. (2003).

Aerosol measurements were performed from a mobile laboratory by the Joint Research Centre, Ispra, Italy. Dry aerosol size distributions in the size range 6–600 nm diameter were measured with a custom built Vienna type differential mobility analyser (DMA), using a TSI CPC model 3010 as particle counter (Thermo Systems Inc. Condensation Particle Counter). The number size distribution of coarse particles was determined with an Optical Particle Counter (OPC, GRIMM model 1.108) in 15 size classes from 300 nm to 10 μm diameter. Note that the aerosols entering the OPC have not been dried, however, for the low relative humidities (<60%) observed during the campaign, the observed aerosol diameter can be regarded as dry diameter. Combining the data of both instruments provides the aerosol size distribution between 6 nm and 10 μm diameter, from which the total aerosol surface area and volume was calculated. Total PM₁₀ (particle diameter (D_p) <10 μm) aerosol mass was obtained on-line with a tapered element oscillating microbalance (TEOM) system, with a total uncertainty of $\pm 15\%$.

4 Meteorology

The synoptic situation over the Canary Islands is usually dominated by a subtropical anticyclone, centred over the Azores (Carslaw et al., 1997). Deviations in the position of this anticyclone generally determine the origin of the airmasses observed at the Izaña observatory. During the MINATROC campaign in July/August 2002 four regions of origin could be identified based on backtrajectories calculated with the HYSPLIT model (HYbrid Single-Particle Lagrangian Integrated Trajectory, <http://www.arl.noaa.gov/ready/hysplit4.html>): north Atlantic, central Atlantic, tropical Africa and the Sahara region.

Several time periods with airmasses containing mineral dust, originating in the Sahara region and tropical Africa could be identified. The strongest Saharan dust plume was observed between 28 and 31 July. Aerosol index images from the TOMS satellite indicate that this dust plume originated in western Algeria and its border region with Mali and Mauritania. Backtrajectory calculations suggest that the airmasses were lifted from between 500 and 1500 m above ground level to the measurement altitude of about 2.5 km, 2.5 to 3 days before arrival at the Izaña measurement station, and originate more to the southwest in Mauritania. Lidar measurements

indicate that the Saharan dust plume extended to an altitude of about 7 km (pers. comm. G. P. Gobbi, 2003).

5 Observations

The mixing ratios of a selection of trace gases together with the observed temperature, relative humidity, aerosol number concentration and aerosol surface area are shown in Fig. 1. Continuous in-situ measurements were performed between 16 July and 15 August 2002. Due to instrument calibrations some short gaps occur in the dataset. A delay in the analytic gas shipment to the measurement station precluded RO_x measurements between 22 July and 29 July. Moreover, due to inlet problems no reliable measurements of acetone, methanol, isoprene and NMHC could be obtained before 29 July. The dataset has been reduced to 30 min averaged values, except for the aerosol mass concentrations for which only hourly averages are available.

Figure 2 shows the average diurnal cycle for a selection of species observed during the campaign. A strong diurnal cycle was observed for most trace gases and the aerosol number concentration. This is mainly driven by local air circulation patterns at the measurement site, which are typical for a high-elevation mountainous site. During daytime the air flows upward to the sampling site resulting from surface warming (upslope winds), while downslope winds are observed during the night, due to cooling of the mountain slopes (Zaveri et al., 1995). As a result, free tropospheric air masses were observed during the night and airmasses influenced by anthropogenic pollution from the local boundary layer during the day.

The fraction of boundary layer air which has been mixed into the free tropospheric airmasses at the measurement station has been estimated using relative humidity profiles obtained by radiosondes launched in Santa Cruz, the capital of Tenerife, situated at the south-western coast of the island (Schultz, 1995). For this method three water vapour mixing ratios are used: (1) the H₂O mixing ratio measured at the Izaña station (H_2O_{iZo}), (2) the H₂O mixing ratio measured by the radiosonde in the free troposphere at the same altitude as the measurement station (H_2O_{FT}) and (3) the H₂O mixing ratio measured by the radiosonde in the marine boundary layer at 100 m a.s.l. (H_2O_{MBL}). The mixing factor can then be defined as: $(\text{H}_2\text{O}_{iZo} - \text{H}_2\text{O}_{FT})/(\text{H}_2\text{O}_{MBL} - \text{H}_2\text{O}_{FT})$. Since only two radiosondes were launched per day only one instantaneous daytime value for the mixing factor could be obtained per day. The daytime mixing factor ranged between –30 and 65% and had a median value of 17% (N=28) in the dust-poor airmasses. During the major dust event the measurements were less influenced by local pollution. Since the dust event lasted for three days, only three numbers for the mixing factor could be determined, namely –30%, 0.8% and 17%, which were all below the median mixing factor of the dust-poor airmasses.

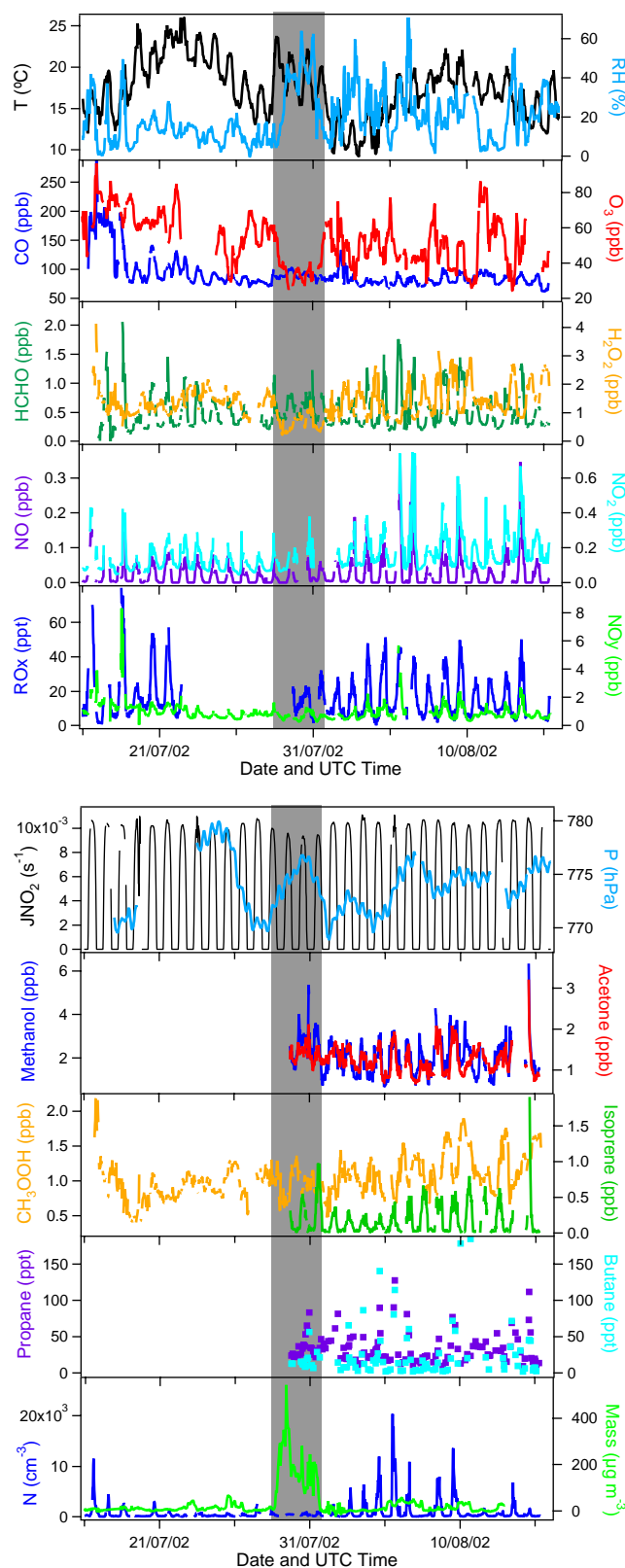


Fig. 1. Time series of the observed meteorological parameters, trace gas mixing ratios and aerosol number and mass concentrations during MINATROC. The major Saharan dust event is marked by the grey area.

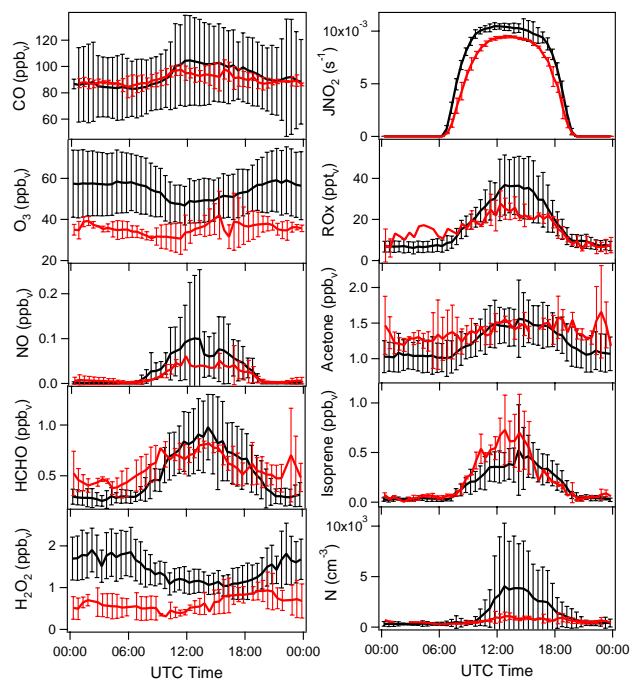


Fig. 2. Diurnal variation of a selection of trace gases and the aerosol number concentration during MINATROC. The red line represents the observations (and 1σ standard deviation) during the major Saharan dust event, the black line the data outside the dust event.

Note that biogenic emissions from vegetation at the slopes of the mountain close to the measurement site influence the observed trace gas mixing ratios at the measurement site in a different manner than anthropogenic emissions, which are transported over a much larger distance from the marine boundary layer. Hence, the calculated mixing factor is a good indicator for the influence of anthropogenic pollution from the marine boundary layer, but not for the influence of more local biogenic emissions.

For CO, NO_x , methanol, acetone and aerosols the upslope winds resulted in an enhancement of the concentrations during the day, due to the intrusion of anthropogenic pollution from the boundary layer. On the other hand O_3 and H_2O_2 mixing ratios were lower during the day, as a result of their positive vertical gradients in the lower atmosphere, mainly due to enhanced destruction of these species by dry deposition at the surface. The RO_x and HCHO mixing ratios closely followed the solar radiation intensity. For these shorter lived species the diurnal variation is less affected by transport and much more dependent on local photochemical production, maximizing around local noon.

For a statistical analysis of the data, upslope and downslope conditions have been separated. Upslope conditions could be identified by a strong enhancement in aerosol number concentration and occurred between 07:00 and 21:00 UTC (daytime), downslope conditions correspondingly between 21:00 and 07:00 UTC (nighttime). Average

Table 2. Average values for meteorological parameters, trace gas mixing ratios and aerosol properties (aerosol number concentration (N), surface area (A), volume (V) and mass) observed during the Saharan dust event and for the dust-poor airmasses. The dataset is subdivided in daytime (upslope) and nighttime (downslope) conditions. Note that VOC and NMHC data are only available after 28 July. For all other parameters data from the entire campaign have been used to determine the average concentrations.

	Daytime		Nighttime	
	dust poor	dust event	dust poor	dust event
Temperature ($^{\circ}\text{C}$)	18.2 ± 3.5	20.0 ± 1.6	15.8 ± 3.3	17.2 ± 1.6
RH (%)	19 ± 11	35 ± 13	16 ± 12	37 ± 15
CO (ppbv)	96 ± 27	92 ± 6	87 ± 29	87 ± 3
O_3 (ppbv)	52 ± 12	35 ± 6	58 ± 15	36 ± 3
HCHO (ppbv)	0.65 ± 0.32	0.64 ± 0.14	0.29 ± 0.08	0.47 ± 0.16
H_2O_2 (ppbv)	1.24 ± 0.38	0.64 ± 0.28	1.72 ± 0.55	0.61 ± 0.25
CH_3OOH (ppbv) ¹	1.0 ± 0.26	0.93 ± 0.16	1.1 ± 0.34	0.99 ± 0.21
NO_x (ppbv)	0.26 ± 0.20	0.17 ± 0.07	0.10 ± 0.04	0.11 ± 0.05
NO_y (ppbv)	1.14 ± 0.75	0.74 ± 0.24	0.77 ± 0.38	0.51 ± 0.20
RO_x (ppt) ²	43 ± 16	28 ± 6	–	–
Methanol (ppbv)	2.35 ± 0.66	2.8 ± 0.5	1.40 ± 0.43	2.3 ± 0.8
Acetone (ppbv)	1.34 ± 0.31	1.4 ± 0.13	1.05 ± 0.23	1.3 ± 0.24
Isoprene (ppbv)	0.27 ± 0.21	0.35 ± 0.26	0.03 ± 0.02	0.05 ± 0.02
Propane (pptv)	41 ± 25	38 ± 15	22 ± 11	34 ± 18
Butane (pptv)	35 ± 37	15 ± 6	13 ± 31	24 ± 28
N (cm^{-3})	1463 ± 2451	551 ± 230	261 ± 186	364 ± 119
A ($\mu\text{m}^2 \text{cm}^{-3}$)	27 ± 23	152 ± 86	16 ± 16	155 ± 54
V ($\mu\text{m}^3 \text{cm}^{-3}$)	3.8 ± 4.1	50 ± 29	3.4 ± 4.7	55 ± 19
Mass ($\mu\text{g m}^{-3}$)	13 ± 14	186 ± 116	12 ± 16	199 ± 61

¹ The CH_3OOH given here is an upper limit for the atmospheric CH_3OOH mixing ratio.

² For RO_x the average daytime maximum mixing ratio is given.

daytime and nighttime values for the observed trace gas mixing ratios and aerosol number concentration, surface area, volume and mass are listed in Table 2.

Table 2 and Fig. 2 also distinguish airmasses containing dust from those which were not influenced by dust. During the measurement campaign several Saharan dust events were probed with PM_{10} aerosol mass concentrations exceeding $25 \mu\text{g m}^{-3}$. The most pronounced dust event was probed between 28 July, 16:45 UTC and 31 July, 15:15 UTC, when aerosol mass concentrations up to $500 \mu\text{g m}^{-3}$ were observed, and the aerosol optical thickness above the measurement station reached values of 0.95. In air masses which were not influenced by Saharan dust, these values were below $10 \mu\text{g m}^{-3}$ and 0.5, respectively. For the analyses in this paper we focus on this major dust event and treat the minor dust events as “dust-poor” airmasses. The time period of the Saharan dust event has been marked by a grey box in Fig. 1.

Some of the observed trace gases show a distinct change during the dust event. The most pronounced is the decrease in ozone mixing ratio from about 65 ppbv just before the dust event started to below 35 ppbv during the

dust event ($\text{ppb}_v = \text{nmol/mol}$). At the same time relatively low H_2O_2 mixing ratios were observed. In free tropospheric air masses (nighttime), an average H_2O_2 mixing ratio of $0.61 \pm 0.25 \text{ ppb}_v$ was observed during the dust period, whereas it was $1.72 \pm 0.55 \text{ ppb}_v$ during the rest of the campaign. Also Fig. 2 depicts significantly lower O_3 and H_2O_2 mixing ratios in airmasses containing dust compared to dust-poor air. Unfortunately no RO_x measurements were available for the first half of the dust period, although during the second part of the dust period lower RO_x peak values, i.e. 23 ppt_v at 30 July and 32 ppt_v at 31 July were observed compared to the dust-poor days ($43 \pm 16 \text{ ppt}_v$). Moreover, a difference in NO_x mixing ratio was found between dust and dust-poor airmasses, which could be a result of the suppressed transport of boundary layer air to the measurement station during the dust event. During upslope conditions 0.17 ppb_v NO_x was found in the dust plume, while 0.26 ppb_v NO_x was observed in the dust-poor airmasses. An additional and possibly more significant effect may be the heterogeneous loss of HNO_3 and N_2O_5 on the dust particles, which indirectly deplete NO_x . The mean relative humidity during the Saharan dust episode was 35%, with peak values up to 60%. This is high compared to the relative humidity observed during the rest of the campaign.

An inhibition of the acetone and methanol diurnal cycle could be observed throughout the dust event, with enhanced mixing ratios during the night, indicating a slightly altered nocturnal wind pattern. On the other hand, enhanced isoprene mixing ratios were found in the dust plume during the day, indicating a greater influence of local biogenic emissions during the dust event. Furthermore, no significant change in the HCHO and CO mixing ratio was observed.

Although a strong decrease in the HNO_3 mixing ratio is expected in a mineral dust plume (e.g. Dentener et al., 1996) and observed by Hanke et al. (2003), no significant change in the NO_y mixing ratio was observed. This is due to the fact that the NO_y converter measures the sum of all gaseous nitrogen species and aerosol nitrate. Hence, the uptake of HNO_3 on mineral dust aerosol is not expected to show up in the NO_y measurements. Remarkably, the mean daytime aerosol number concentration is highest in the dust-poor airmasses, which may also be explained by a reduced mixing of boundary layer air in the dust plume. The much higher particle surface area and mass concentration observed during the dust event indicates a very different aerosol size distribution in the dust loaded airmasses, with a higher number of larger particles. The small particles are probably scavenged by the larger Saharan dust aerosols in the plume, reducing the total aerosol number concentration. The photolysis rates of O_3 and NO_2 are reduced in the dust plume due to the absorption and scattering of solar radiation by the dense aerosol. The average daytime JNO_2 photolysis rate decreased by 17% and JO^1D by 15% during the Saharan dust event compared to the rest of the campaign.

Table 3. Comparison of the median daytime and nighttime (day/night) trace gas mixing ratios during the MINATROC campaign at Izaña and at Mt. Cimone and during the OCTA campaign at Izaña in July/August 1993. For RO_x only a mean noontime value is given. Only the dust-poor data from MINATROC is used for this comparison.

	Izaña	Mt. Cimone ¹	Izaña ²
Field campaign	MINATROC	MINATROC	OCTA
Time period	July/August 2002	June 2000	July/August 1993
O_3 (ppb_v)	52/59	56/60	38/40
CO (ppb_v)	88/78	119/118	92/89
NO_x (ppt_v)	210/95	267/197	76/47
NO_y (ppb_v)	0.95/0.66	0.90/1.0	0.52/0.39
HCHO (ppb_v)	0.58/0.29	1.4/1.1	1.4/1.1
H_2O_2 (ppb_v)	1.17/1.63	n.a.	2.1/2.4
RO_x (ppt_v)	43	31	65

¹ Fischer et al. (2003)

² Fischer et al. (1998)

Another interesting observation is the very high CO and O_3 mixing ratios during the first two days of the measurement campaign, which could be attributed to long range transport of a biomass burning plume from large forest fires in Quebec, Canada, on 6–9 July 2002. During these two days CO mixing ratios as high as 290 ppb_v and O_3 mixing ratios of 100 ppb_v were observed. Although very interesting, this period will not be further studied in this paper.

A comparison of the observed trace gas mixing ratios with observations made during the first MINATROC field campaign on Mt. Cimone in June 2000 (Fischer et al., 2003) is presented in Table 3. The Mt. Cimone station is situated at 2165 m a.s.l. on the highest mountain in the northern Italian Apennines ($44^\circ 11' \text{ N}$, $10^\circ 42' \text{ E}$). Due to its location in southern Europe, the sampled airmasses represent European continental background conditions. Similar O_3 mixing ratios have been observed at both measurements sites, while the CO and NO_x mixing ratios were slightly lower at Izaña, indicative of a more remote site, though influenced by continental pollution. The HCHO mixing ratios observed at Izaña were, however, much lower than those observed at Mt. Cimone. The results from the MINATROC campaign are also compared with measurements at the Izaña observatory performed in July/August 1993 during the OCTA field campaign (Fischer et al., 1998). Compared to the measurements at the same site nine years earlier, slightly higher O_3 and NO_x mixing ratios and much lower HCHO and H_2O_2 mixing ratios were observed in 2002. This appears to be consistent with an upward O_3 trend observed downwind of western Africa (Lelieveld et al., 2004). The median nighttime CO mixing ratio in 2002 was 9 ppb_v lower than that observed in 1993, in line with the observed CO trend of $-0.92 \pm 0.15 \text{ ppb}_v/\text{yr}$ in the northern hemisphere lower troposphere (Novelli et al.,

2003). The observed RO_x mixing ratios were similar, taking into account the large uncertainty in the RO_x measurements.

6 Boxmodel calculations

To investigate photochemistry, net ozone production and the influence of Saharan dust aerosol on the mixing ratios of peroxy radicals, formaldehyde and hydrogen peroxide, model calculations were performed with the chemistry box model MECCA (Module Efficiently Calculating the Chemistry of the Atmosphere). The chemical reaction scheme has been adopted from von Kuhlmann et al. (2003) and includes detailed chemistry of organic species with up to four C-atoms and isoprene (Sander et al., 2004). The reaction rates have generally been adopted from the Jet Propulsion Laboratory (JPL) 2003 database (Sander et al., 2003). Heterogeneous removal reactions of HO_2 and H_2O_2 on mineral dust have been added to the chemical scheme, analogous to de Reus et al. (2000). In total 67 chemical species, 110 gas phase chemical reactions, 34 photolysis reactions and 2 heterogeneous removal reactions were included (see electronic supplement).

The boxmodel has been employed by constraining the concentrations of relatively long-lived trace gases to the observed values (see next section for a detailed description), whereas the steady state concentrations of short-lived trace gases are calculated. Here, we focus on peroxy radicals, formaldehyde and hydrogen peroxide.

6.1 Input parameters

Since two sets of observations are available per hour, a model simulation is started every 30 min. Each simulation has been initialised with the observed temperature, pressure, O_3 , CO , H_2O , NO , H_2O_2 , CH_3OOH , acetone, methanol, isoprene, propane and butane mixing ratios, which are shown in Fig. 1. Short gaps for which data are missing have been filled through interpolation. HNO_3 is initialised using the observed NO_z mixing ratio ($\text{NO}_z = \text{NO}_y - \text{NO}_x$). Since NO_y also includes atmospheric aerosol nitrate, HNO_3 will likely be strongly overestimated during the dust event when NO_z is used as a proxy for HNO_3 (see Sect. 5). Therefore, HNO_3 is set to zero during the major Saharan dust event. For CH_4 and CO_2 background mixing ratios for the year 2002 of 1.75 and 372 ppm_v have been used, respectively. Since no measurements of ethane, ethene and propene were performed during MINATROC, the mixing ratios of these species were scaled to the observed propane mixing ratio using the mean daytime mixing ratios observed during a former campaign at Izaña in July/August 1993 (Fischer et al., 1998). During this campaign the mean ratios of ethane, ethene and propene to propane were 10, 0.6 and 0.2, respectively.

JO^1D and JNO_2 photolysis rates were measured during the campaign and have been used as reaction rates for the photolysis reaction of O_3 (to O^1D) and NO_2 , respectively.

Other photolysis rates have been calculated using the Tropospheric Ultraviolet-Visible (TUV, version 4.1) radiation model (Madronich and Flocke, 1998). For these calculations, the total ozone column measured with a Dobson spectrometer at the Izaña station has been used as input value, while default values for the SO_2 , NO_2 , cloud and aerosol optical depth were used. To account for cloud overpasses and the reduction of solar radiation due to the Saharan dust plume, the calculated photolysis rates have been scaled to the ratio of the measured to the calculated JNO_2 photolysis rates.

A model simulation has been performed for every 30 min data point during daytime hours (solar zenith angle $< 70^\circ$). The mixing ratios of the above listed trace gases, temperature, pressure and photolysis rates have been kept constant during each simulation, while the model was run for 10 days, to make sure that steady state was achieved. Since no VOC and NMHC data are available before 29 July, only the later part of the campaign has been analysed.

6.2 Gas phase chemistry

Before we performed model simulations for the MINATROC dataset, we first carried out some calculations to determine the time needed to reach steady state for different species. We defined the steady state time as the time the boxmodel needs to reach a mixing ratio which did not change more than 1% in the last 30 min. The steady state time has been determined for different solar zenith angles during a randomly chosen day during the campaign. When no isoprene is included in the model calculations, steady state concentrations of HCHO and RO_x were reached after 9 and 6 h, respectively, at local noon and after 33 h for H_2O_2 . At a solar zenith angle of 70° , steady state mixing ratios were reached within 10, 7 and 52 h for HCHO, RO_x and H_2O_2 , respectively. For larger solar zenith angles a steady state HCHO, RO_x and H_2O_2 mixing ratio could not be reached at all. Therefore, the simulations are limited to time periods during which the solar zenith angle is less than 70° (08:15–18:15 UTC), and each model simulation continues for 10 days, to ensure that steady state is achieved.

Running the model for 10 days instead of the above defined steady state time does not lead to significantly different results, since the mixing ratios of HCHO, RO_x and H_2O_2 do not change much after this point. For RO_x and HCHO the difference between the above defined steady state concentration and the concentration after 10 days of simulation is smaller than 1%. For H_2O_2 differences up to 8% at high solar zenith angles can be found.

6.2.1 Reference run

The RO_x mixing ratio calculated by the model without heterogeneous chemistry, for the period 29 July to 15 August 2002, is shown in Fig. 3a. RO_x is the sum of HO_2 , CH_3O_2 , higher organic peroxy radicals with up to 4 C atoms and

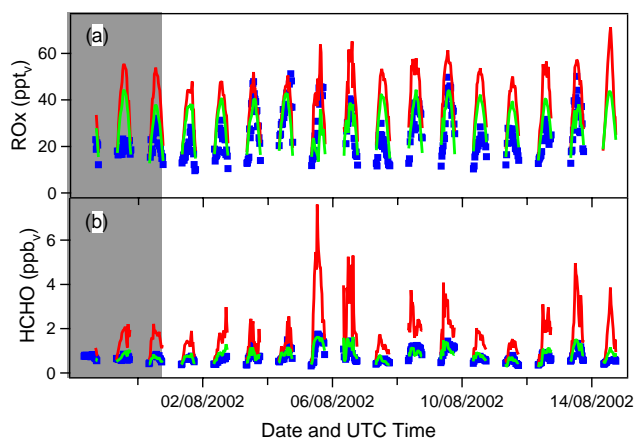


Fig. 3. Observed (blue dots) and modelled (red solid line, reference run) RO_x and HCHO mixing ratios. The green solid line represents the model calculation without isoprene. The major Saharan dust event is marked by the grey area.

peroxy radicals formed during isoprene degradation. The main constituents of the modelled RO_x are HO_2 (60%), CH_3O_2 (18%) and the peroxy radicals from isoprene degradation (16%). The contribution of other higher organic peroxy radicals to the total RO_x is very small, on average $\text{C}_2\text{H}_5\text{O}_2$ contributes 0.06% to the total modelled RO_x , $\text{C}_2\text{H}_3\text{O}_3$ 5.6%, $\text{C}_3\text{H}_7\text{O}_2$ 0.01%, $\text{C}_3\text{H}_6\text{O}_2$ 0.17%, $\text{C}_3\text{H}_5\text{O}_3$ 0.08%, $\text{C}_4\text{H}_9\text{O}_2$ 0.02% and $\text{C}_4\text{H}_9\text{O}_4$ 0.003%. The RO_x mixing ratio is clearly overestimated by the model, and the mean ratio of the calculated to the observed RO_x mixing ratio (RO_x calc/obs) is 1.70.

Figure 3b shows the calculated and observed HCHO mixing ratios. The HCHO mixing ratios are also strongly overestimated by the model. The daytime maximum HCHO mixing ratio calculated by the model ranges between 1.5 and 7.5 ppbv, while the observed values vary between 0.7 and 1.7 ppbv. The mean ratio of the calculated to observed HCHO mixing ratio (HCHO calc/obs) equals 2.29, however, a good correlation can be found between the observed and calculated HCHO mixing ratios. When fitting a straight line through the data points, the correlation coefficient r is 0.80.

Possible reasons for the model overestimation of both the RO_x and HCHO mixing ratios could either be an underestimation of the observed HCHO and RO_x mixing ratios, an overestimation of the precursor gas concentrations, which are used as input for the calculations or unknown model errors. Moreover, the assumption that the air mass is in steady state might be erroneous.

A comparison of the HCHO and RO_x mixing ratios with a previous measurement campaign at Izaña shows that the HCHO mixing ratios are a factor 2 lower than those observed nine years earlier, however, during this campaign the HCHO measurements were probably overestimated due to a spectral interference to CH_4 (Fischer et al., 1998). The RO_x mixing

Table 4. Calculated RO_x and HCHO mixing ratios and calculated/observed ratios for the sensitivity runs in which the mixing ratio of the trace gas in column 1 has been reduced by a factor 2 compared to the reference run.

	RO_x (ppt _v)	RO_x calc/obs	HCHO (ppb _v)	HCHO calc/obs
Reference run	40	1.70	1.81	2.29
O_3	36	1.52	1.63	2.03
CO	41	1.72	1.86	2.34
H_2O	37	1.58	1.69	2.12
NO	38	1.62	1.22	1.55
Methanol	40	1.70	1.80	2.27
Acetone	40	1.69	1.80	2.27
HNO_3	40	1.70	1.81	2.28
H_2O_2	40	1.67	1.79	2.25
CH_3OOH	39	1.65	1.72	2.16
Isoprene	36	1.53	1.43	1.83
NMHC	40	1.70	1.81	2.28

ratios are similar considering the large uncertainty in the RO_x measurements (see Table 3). The influence of the input concentrations of different precursor gases for HCHO and RO_x will be studied in the next section.

6.2.2 Sensitivity simulations

To investigate the effects of a range of model input parameters, several sensitivity studies have been performed in which the mixing ratio of one trace gas has been reduced by a factor two compared to the reference run. The results are summarised in Table 4.

The calculated RO_x mixing ratio is rather insensitive to the changes in the input mixing ratios of most trace gases, except for O_3 and H_2O , which are direct precursors of HO_2 , and for isoprene, which is a main precursor for different organic peroxides. Since the organic peroxy radicals, not originating from isoprene, contribute only 6% to the total peroxy radical mixing ratio, changes in the higher hydrocarbon concentrations do not have a significant effect on the calculated RO_x mixing ratio.

The simulated HCHO mixing ratio is more variable, and especially sensitive to the input concentration of NO. A reduction of the NO mixing ratio by a factor 2 causes the HCHO mixing ratio to decrease by 33%. At low NO mixing ratios the production of HCHO mainly occurs via the reaction of HO_2 with CH_3O_2 and the subsequent photolysis of CH_3OOH , while at higher NO mixing ratios, the HCHO production is dominated by the faster reaction of CH_3O_2 with NO, leading to an enhanced production of HCHO.

The simulated HCHO mixing ratio is also sensitive to the input concentration of isoprene (21% reduction of HCHO when the isoprene mixing ratio is reduced with a factor 2),

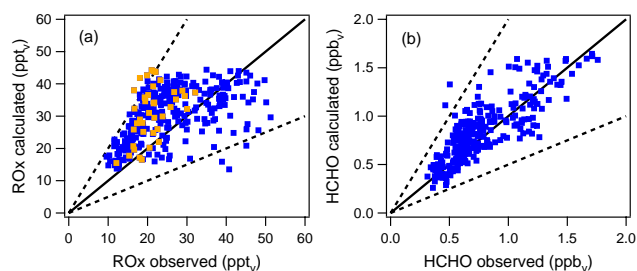


Fig. 4. Comparison between the calculated and observed RO_x (a) and HCHO (b) mixing ratios (blue dots) for the model run without isoprene. The orange dots represent the RO_x mixing ratios during the major Saharan dust event. The solid black line represents the 1:1 relationship, the dashed lines the 1:2 and 2:1 relationships.

O₃ (10%), H₂O (7%) and CH₃OOH (5%). Isoprene and CH₃OOH are precursor gases of HCHO, so a reduction in the mixing ratio of these trace gases will directly result in a reduced HCHO production. O₃ and H₂O influence the HCHO mixing ratio through the change in OH mixing ratio. If the concentration of O₃ or H₂O is reduced, less OH is produced via the reaction of H₂O with O¹D and less OH will be available for the destruction of VOCs and notably isoprene, which results in a reduced production of HCHO.

The above described sensitivity studies show that the RO_x and HCHO mixing ratios are most sensitive to the mixing ratio of NO, O₃, H₂O, CH₃OOH and isoprene. From these gases, the measurement uncertainty, and hence the uncertainty of the boxmodel input mixing ratios, of isoprene and CH₃OOH is the largest.

As has been discussed in the observations section, the isoprene mixing ratio is probably determined by emissions close to the measurement station. Therefore, the airmass may not have reached equilibrium with respect to isoprene. We intend to calculate the equivalent isoprene mixing ratio, which corresponds to the observed HCHO and RO_x mixing ratios. While doing so we found that a simulation without taking isoprene into account provides the best agreement with the measurements, indicating that isoprene may not have a significant effect on the observed HCHO and RO_x mixing ratio and that the effect of the emissions of isoprene (and other biogenic compounds) on the HCHO budget will first show up during further evolution of the airmass.

Moreover, the isoprene mixing ratios observed during MINATROC were high relative to the isoprene mixing ratios observed during the OCTA campaign at Izaña in July/August 1993 (Fischer et al., 1998). Excluding the measurements performed during the major dust event, the mean isoprene mixing ratio was 270 ± 206 ppt_v during the day and below the detection limit at night. This is a factor 4.5 higher than the mean daytime isoprene mixing ratio observed during OCTA, which was 60 ± 124 ppt_v (Fischer et al., 1998).

Putting the isoprene mixing ratio to zero leads to decreases in both the HCHO and RO_x mixing ratios. The mean calc/obs ratio of RO_x decreases from 1.70 in the reference run to 1.31

in the run without isoprene. The contribution of the different peroxy radicals to the total RO_x mixing ratio changes, since no organic peroxy radicals are formed during the isoprene degradation. The main constituents of RO_x are still HO₂ (72%) and CH₃O₂ (26%), while the contribution of other organic peroxy radicals decreases to 2%. The effect of isoprene on the HCHO mixing ratio is even stronger than on RO_x. The calc/obs ratio of HCHO decreases from 2.29 in the reference run to 1.12 in the run without isoprene.

A detailed comparison between the observed and modelled RO_x mixing ratios is shown in Fig. 4a. Here the solid line represents the ideal 1:1 relationship between the modelled and observed values, while the dashed lines correspond to a deviation of this ideal relationship by a factor of 2, which about equals the total uncertainty of all measured parameters used as input for the model calculations. In total 304 model data points could be used for the comparison with observations, from which 97% agree within a factor of two. A straight line fit through the calculated and observed RO_x mixing ratios gives a linear correlation coefficient r of 0.50.

The diurnal variation and the absolute mixing ratios of HCHO are captured well by the model (see Fig. 3b). On average the model slightly overestimates the HCHO mixing ratio, the mean ratio of the calculated HCHO mixing ratio to the observed HCHO mixing ratio (HCHO calc/obs) is 1.12. From the 272 data points, 99% of the calculated HCHO mixing ratios are within a factor two of the observed HCHO mixing ratios (see Fig. 4b). Moreover, a good correlation is found between the observed and calculated HCHO mixing ratios. When fitting a straight line through the data points in Fig. 4b, the correlation coefficient r is 0.82.

Previous model studies using three dimensional global chemistry-transport or boxmodels have also investigated the HCHO budget. The comparison between modelled and observed HCHO concentrations provides very different results. In the remote marine boundary layer (Ayers et al., 1997; Weller et al., 2000) and the upper free troposphere (Korrmann et al., 2003; Jaegle et al., 2000) models tend to underestimate the concentration of HCHO. For the above mentioned marine boundary layer calculations this could at least partly be explained by a lack of higher hydrocarbons in the model, however, for the upper troposphere including higher hydrocarbons did not reproduce the high concentrations observed. For the polluted marine boundary layer and the lower free troposphere HCHO mixing ratios are generally overestimated by models (e.g. Wagner et al. 2002; Zhou et al., 1996). Possible explanations for the overprediction of HCHO by models are deficiencies in considering dry deposition, multiphase chemistry in aerosols and clouds or halogen chemistry in the marine boundary layer. On the other hand, Olson et al. (2004) found a good agreement between observed and modelled HCHO mixing ratios between 60 and 500 ppt_v in the free troposphere. At higher HCHO concentrations the model increasingly underpredicts HCHO, which could be explained by the transport of very polluted airmasses.

To investigate the effect of dry deposition in our simulations we included a sinusoidal dry deposition rate for HCHO analogous to H_2O_2 , which is explained in detail in the next section. A noon time maximum dry deposition rate of $8.4 \times 10^{-7} \text{ s}^{-1}$ is necessary to achieve good agreement between the calculated and observed HCHO mixing ratios. This is more than the dry deposition rate necessary to explain the H_2O_2 measurements (see next section). Based on the difference in solubility and reactivity, the dry deposition velocity of H_2O_2 should at least be a factor 2 higher than HCHO (L. Ganzeveld, pers. comm., 2004), hence dry deposition can only partly explain the difference between model and observations.

6.2.3 Discussion

In this section we will discuss if the setup of the boxmodel is appropriate for the model simulations which are presented in this work. We will focus on the following three questions. Is it realistic to assume that the airmass is in steady state, when it takes the model up to 10 h to reach a steady state mixing ratio for HCHO and RO_x ? Wouldn't it be more appropriate to include a diurnal cycle of the photolysis rates, so that the photochemical components are simulated in a more realistic way? Why is the temporal development of the trace gases not taken into account during the simulations?

The model is used to calculate steady state concentrations and not to simulate the history of the airmass. By keeping the concentrations of relatively long lived trace gases and the photolysis rates constant we tried to simulate the "potential" concentrations of the gases when the airmass would have been in photochemical steady state. So we do not intend to perform a lagrangian simulation.

The definition of steady state time used in this paper is very harsh. Compared to the uncertainty of the measurements and the model a change of 1 in 30 min is very small. Nevertheless, steady state mixing ratios of HCHO and RO_x could be reached within a day.

The airmasses arriving at the measurement station originate partly from the free troposphere and partly from the marine boundary layer. On average the contribution of the marine boundary layer was 17%. It is realistic to assume that the mixing ratios of the long lived trace gases, which are used as input for the boxmodel, in the free tropospheric airmass do not change dramatically within 6–10 h. The marine boundary layer airmass, however, is subject to anthropogenic emissions in the coastal area and to biogenic emissions closer to the measurement site. We could show that the airmass was probably not in steady state with respect to isoprene, which has been emitted close to the measurement station, and that removing isoprene from the calculations did improve the agreement between observations and boxmodel calculations. Considering the average wind speed and wind direction of the measurement station during MINATROC, the average transport time of the airmass from the marine

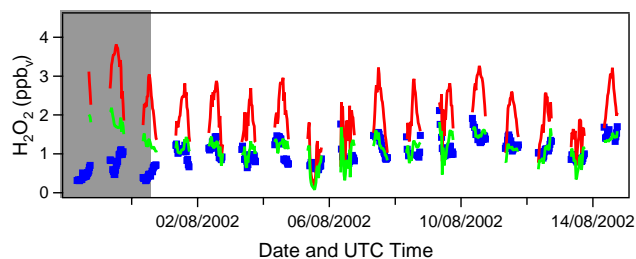


Fig. 5. Observed (blue dots) and calculated (red solid lines) H_2O_2 mixing ratios for the model run in which the mixing ratios of H_2O_2 are not fixed to the observed values. The green solid line represents the model run in which dry deposition of H_2O_2 is included. The major Saharan dust event is marked by the grey area.

boundary layer to the measurement station is estimated to be 1.5 h. After 1.5 h of simulation the RO_x mixing ratio reached 93% of its end mixing ratio (after 10 days of simulation) and HCHO 69%. Taking into account the average contribution of marine boundary layer air of 17%, we estimated an uncertainty of 5% and 1% for HCHO and RO_x , respectively, due to this possible non steady state.

These numbers also show the uncertainty of the model simulations early during the day. 1.5 h after sunrise the steady state RO_x mixing ratio was reached by 93% and HCHO by 69% providing an uncertainty of 7% and 31% for RO_x and HCHO, respectively. Note that the first simulations we presented were at 08:15 UTC, which is about 2 h after sunrise.

In a further development of the boxmodel a diurnal cycle of the photolysis rates has been implemented, analogous to the work of Olson et al. (2004), to account for the diurnal cycle of photochemical components. From these simulations a diurnal steady state mixing ratio can be determined. With this setup of the model the NO mixing ratio cannot be fixed but a diurnal emission pattern had to be included so that the resulting NO concentration was similar to the observed concentration. First tests with the new setup of the model for another measurement campaign, did not show large differences between the two approaches (fixed photolysis rates or a diurnal cycle in the photolysis rates), however this comparison has been done for a single model run in the upper troposphere, and provides no statistically significant results.

6.2.4 Simulation of hydrogen peroxide

Since we focus on the ability of the model to simulate observed H_2O_2 mixing ratios, a model simulation has been performed in which H_2O_2 is not fixed to the measured mixing ratio but has been calculated freely by the model. For this, the model run without isoprene is taken as a reference. The results of this simulation are shown in Fig. 5. The H_2O_2 mixing ratio calculated by the model is much higher than the observed H_2O_2 mixing ratio ($\text{H}_2\text{O}_2 \text{ calc/obs}=2.16$). This is

mainly due to the fact that dry deposition of H_2O_2 at the surface is not included in the model.

The discrepancy between the calculated and observed values is largest during the Saharan dust event. Due to the high relative humidity observed during this period, relatively high H_2O_2 mixing ratios are calculated, while much lower mixing ratios were observed. Excluding the dust data points from the total dataset gives a much better agreement between observed and calculated values. For the dust-poor period, the mean calc/obs ratio of H_2O_2 is 1.75.

To improve the agreement between the observed and modelled values, we included a sinusoidal dry deposition rate for H_2O_2 in the model, with the highest deposition rate at local noon, when the upslope winds and turbulent exchange in the boundary layer are relatively strong. Dry deposition was parameterised such that after each steady state calculation the concentration of H_2O_2 was reduced according to this dry deposition rate. A calc/obs ratio of H_2O_2 of one was obtained (for the dust-poor period) when a maximum dry deposition rate of $6.5 \times 10^{-7} \text{ s}^{-1}$ at local noon was assumed, corresponding to a removal fraction of 56%. For the complex meteorological situation at the measurement station with mixing of boundary layer air, which is subject to dry deposition and free tropospheric air, which is likely not influenced by dry deposition, it is difficult to translate this dry deposition rate into a deposition velocity. The results of this simulation are also presented in Fig. 5. From this figure it is clear that even if dry deposition is included in the model calculations, the H_2O_2 mixing ratio is still strongly overestimated during the major Saharan dust event. A reason for this may be the uptake of H_2O_2 and/or HO_2 on the surface of the dust aerosols, which will be investigated in the next section.

6.3 Heterogeneous chemistry

The observations during the Saharan dust event show reduced mixing ratios of RO_x and H_2O_2 . The reduced H_2O_2 mixing ratios could not be explained by gas phase chemistry or through the reduction in photolysis rates. Even after including dry deposition the model strongly overestimates the H_2O_2 mixing ratios during the dust event. Also the RO_x mixing ratios are overestimated by the (gas phase) model during the dust event, however, there is no clear relation with the presence of Saharan dust. To investigate the influence of Saharan dust aerosol particles on the mixing ratio of peroxy radicals and hydrogen peroxide, heterogeneous uptake reactions of HO_2 and H_2O_2 have been included in the model. Note that radiation effects of mineral dust aerosol have been accounted for by the scaling of the photolysis rates to the observed JNO_2 value.

6.3.1 Heterogeneous removal reactions

The removal rate of gas-phase species j by aerosol particles can be described by a pseudo-first-order rate coefficient k_j

(s^{-1}), given by Heikes and Thompson (1983):

$$k_j = \int_{r_1}^{r_2} k_{d,j}(r)n(r)dr \quad (1)$$

where $n(r)dr$ (cm^{-3}) represents the number concentration of particles with a radius between r and $r+dr$, and $k_{d,j}(r)$ is the size dependent mass transfer coefficient ($\text{cm}^3 \text{ s}^{-1}$), which can be calculated using the Fuchs and Sutugin (1970) interpolation equation:

$$k_{d,j} = \frac{4\pi D_j V}{1 + Kn(x + 4(1 - \alpha)/3\alpha)} \quad (2)$$

where D_j ($\text{cm}^2 \text{ s}^{-1}$) is the gas phase molecular diffusion coefficient of species j , V the ventilation coefficient, which is close to unity, and Kn the dimensionless Knudsen number, defined as the ratio of the effective mean free path of a gas molecule in air, λ , to the particle radius r . α is the mass accommodation coefficient, a dimensionless number defined as the number of molecules adsorbed by the surface of an aerosol divided by the number of collisions with the aerosol; x represents a correction factor for anisotropic movement and is dependent on the Knudsen number (Fuchs and Sutugin, 1970).

In the laboratory much effort has been undertaken to determine the reactive uptake coefficient (γ) of different atmospheric gases on mineral dust aerosol (e.g. Usher et al., 2003; Hanisch and Crowley, 2003; Underwood et al., 2001). The reactive uptake coefficient represents the fraction of collisions with a particle that leads to irreversible loss of the gas (thus including chemical reactions). For the calculation of the heterogeneous removal rate the accommodation coefficient α needs to be known, denoting the probability that a gas molecule, colliding with an aerosol particle, will be (physically) incorporated into the particle. Since we do not explicitly account for chemical reactions in the condensed phase, we substitute α by γ . Since γ is a measure for the net transfer of the species to the aerosol particle, α represents an upper limit of γ .

Unfortunately no laboratory studies of the uptake of the HO_2 radical on mineral dust aerosol are documented, however, a few studies are performed to determine the uptake of HO_2 on different types of surfaces. Hanson et al. (1992), for example, determined the uptake of HO_2 on a water and sulphuric acid surface and found reactive uptake coefficients of >0.01 and >0.05 , respectively, while Cooper and Abbatt (1996) measured net uptake coefficients for HO_2 radicals on supercooled sulphuric acid water-ice surfaces of 0.055 and 0.025, respectively. The presence of free Cu ions in the aerosol enhances the uptake of HO_2 on aqueous surfaces significantly (Mozurkewich et al., 1987). In a review Jacob (2000) concludes that the uptake of HO_2 by aqueous aerosols takes place with a γ of 0.1–1, and he recommends including the uptake of HO_2 by aerosols with $\gamma=0.2$ in atmospheric

chemistry models. This is also the value of γ we deploy in this study. The author also concludes that although the mechanism for HO_2 uptake is uncertain, H_2O_2 is the likely product (Jacob, 2000).

Even fewer laboratory studies have been conducted on the uptake of H_2O_2 on different types of surfaces. Worsnop et al. (1989) determined the mass accommodation coefficient of H_2O_2 on aqueous surfaces. They found a strong negative temperature dependence of the mass accommodation coefficient, with an uptake coefficient of 0.18 ± 0.02 at 273 K. Clegg and Abbatt (2001) determined the absolute uptake of H_2O_2 on an ice surface to be 4×10^9 molecules cm^{-2} , at an average ambient H_2O_2 mixing ratio of about 1 ppbv. For the maximum aerosol surface area of $500 \mu\text{m}^2/\text{cm}^3$ observed during the major Saharan dust event during MINATROC, this will cause a negligible decrease in H_2O_2 mixing ratio of much less than 1%. To our knowledge no laboratory studies on the uptake of H_2O_2 on mineral dust aerosol have been performed, therefore, different uptake coefficients will be tested in this study, starting with the value of 0.18.

The heterogeneous removal rate for HO_2 and H_2O_2 has been calculated off-line using the observed aerosol size distribution, temperature and pressure. For this, the complete size range from 6 nm to $10 \mu\text{m}$ has been taken into account.

Trajectory analyses indicate that the dust-loaded air masses travelled about 3 days from the source region in Africa (western Algeria and Mauritania) to the measurement station. To calculate a realistic uptake coefficient we have to use a realistic time for dust uptake. Therefore, heterogeneous removal reactions were only activated the last three days of the simulation. We realise that here we mix up the steady state and lagrangian approach of the boxmodel.

6.3.2 Results of heterogeneous chemistry calculations

To find the accommodation coefficient for the heterogeneous uptake of H_2O_2 on Saharan dust particles we altered the H_2O_2 accommodation coefficient until the calc/obs ratio of H_2O_2 was equal to one. For this all data points starting at 29 July were used and dry deposition, as described in Sect. 6.2.3, was included. When the uptake coefficient for aqueous surfaces is used ($\gamma=0.18$) almost all H_2O_2 is scavenged and the calc/obs ratio of H_2O_2 decreases to 0.04. A calc/obs ratio of H_2O_2 of one was found for a much lower accommodation coefficient, 5×10^{-4} . The corresponding average removal rate of H_2O_2 , k_j , during the major dust event was $8 \times 10^{-6} \text{ s}^{-1}$. The results of the simulation with this accommodation coefficient are shown in Fig. 6a. From the 265 data points 93% of the modelled H_2O_2 mixing ratios were within a factor of 2 of the observed mixing ratio.

The influence of the reduced H_2O_2 mixing ratios on RO_x appears to be relatively small; the calc/obs ratio of RO_x decreases from 1.38 in the run without heterogeneous removal reactions to 1.36 in the run with H_2O_2 scavenging. Hence, the reduced RO_x mixing ratios observed during the dust event

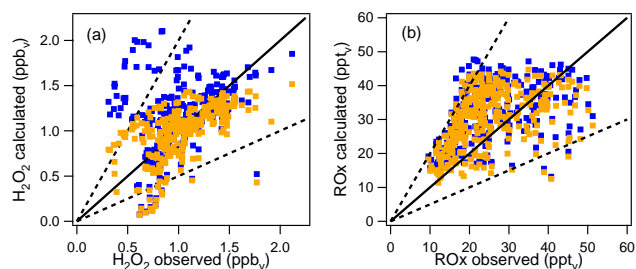


Fig. 6. Comparison between the calculated and observed H_2O_2 and RO_x mixing ratios (blue dots). The orange dots represent the model run including heterogeneous removal of (a) H_2O_2 ($\gamma=5 \times 10^{-4}$) and (b) HO_2 ($\gamma=0.2$) on Saharan dust aerosol. The solid black line represents the 1:1 relationship, the dashed lines the 1:2 and 2:1 relationships.

cannot be explained by heterogeneous removal of H_2O_2 on Saharan dust aerosol. Therefore, we investigated the effect of heterogeneous removal of HO_2 on Saharan dust particles on the RO_x mixing ratio. For this an uptake coefficient of 0.2 is assumed, according to the recommendation of Jacob (2000), corresponding to a first order rate coefficient, k_j , of $2 \times 10^{-3} \text{ s}^{-1}$ during the major dust event. Two simulations were performed: one in which the HO_2 is irreversibly removed by the dust aerosols, and one in which one molecule of H_2O_2 is produced on the surface of a dust particle for each molecule HO_2 which is taken up.

In spite of the relatively high uptake coefficient, heterogeneous removal of HO_2 causes only a small decrease in the RO_x mixing ratio. The calc/obs ratio of RO_x decreases from 1.38 in the run without heterogeneous removal reactions to 1.30 in the run with heterogeneous removal of HO_2 (see Fig. 6b). Even when an uptake coefficient of 1 is assumed the model still overestimates the RO_x mixing ratio ($\text{RO}_x \text{ calc/obs}=1.14$). The relatively small change in the calculated RO_x mixing ratio indicates that the heterogeneous removal reaction of HO_2 is slow compared to the fast gas phase production and destruction reactions of HO_2 . The effect of heterogeneous removal of HO_2 on the H_2O_2 mixing ratio, however, is very strong. The H_2O_2 mixing ratio decreases to almost the observed value ($\text{H}_2\text{O}_2 \text{ calc/obs}=1.05$) when heterogeneous removal of HO_2 with an uptake coefficient of 0.2 is included in the model. Hence, if no H_2O_2 is formed during the uptake reaction of HO_2 on Saharan dust particles, only including heterogeneous removal of HO_2 leads to a good agreement between the calculated and observed H_2O_2 mixing ratios. Note that a calc/obs ratio of H_2O_2 of exactly one is reached when heterogeneous removal of H_2O_2 with an accommodation coefficient of 7×10^{-5} is additionally included in the model.

If we assume that H_2O_2 is formed when HO_2 is taken up in the Saharan dust aerosol the H_2O_2 mixing ratio increases strongly compared to the run without heterogeneous chemistry, while the effect on RO_x is marginal. During the major

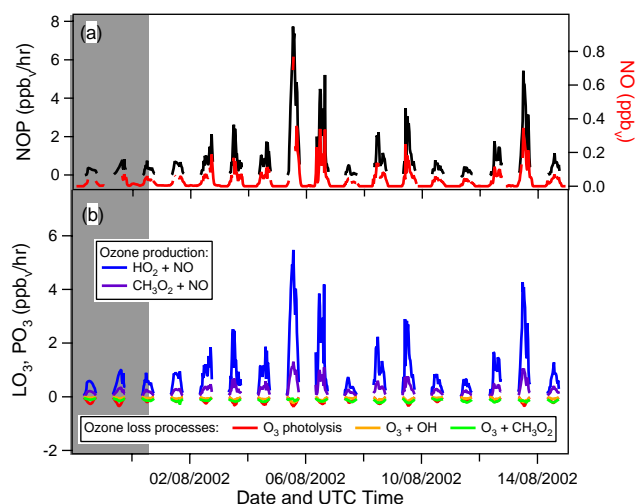


Fig. 7. Calculated net ozone production rate (NOP) for the MINATROC campaign (a) and partitioning of the different production and loss processes (b). The major Saharan dust event is marked by the grey area.

dust event the calculated H_2O_2 mixing ratio exceeds 5 ppbv , and an average calc/obs ratio of H_2O_2 of 1.89 is calculated. Heterogeneous removal of H_2O_2 with an accommodation coefficient of 2×10^{-3} had to be included to restore the agreement between calculated and observed values.

6.4 Ozone production rates

The model calculations have been set up to calculate the steady state concentrations of relatively short lived trace gases, while the observed mixing ratios of longer lived species, including ozone, were used as input parameters. This precludes the comparison of calculated and observed O_3 mixing ratios, and drawing conclusions about for example ozone uptake on Saharan dust particles. This would require a model calculation along a back-trajectory, however, the concentration values needed to constrain the model over the dust source region are not available.

Instead, we focus on the calculation of the net ozone production rate (NOP) during the campaign, to try to explain the low ozone mixing ratios observed during the major dust event by changes in the ozone production and loss rates. The method to determine the NOP has been introduced by Liu et al. (1980) and is summarised below. A detailed description of the procedure can also be found in Fischer et al. (2003) for the first part of the MINATROC project.

The net ozone production rate can be described as the difference between the ozone production ($\text{PO}_3 = \{k_1[\text{HO}_2] + k_2[\text{CH}_3\text{O}_2]\}[\text{NO}]$) and loss rates ($\text{LO}_3 = (f \times \text{JO}^1\text{D} + k_3[\text{OH}] + k_4[\text{HO}_2]) [\text{O}_3]$), where k_1 and k_2 are the reaction rates of the reaction of NO with HO_2 and CH_3O_2 , respectively, f is the fraction of O^1D atoms reacting with H_2O to produce OH rather than being deactivated through collisions with air molecules, JO^1D is

the photolysis rate of O_3 , and k_3 and k_4 are the reaction rates of the reaction of O_3 with OH and HO_2 , respectively. In this approach, it is assumed that ozone loss due to dry deposition, heterogeneous reactions, uptake in cloud droplets and reactions with unsaturated VOCs are negligible.

The mixing ratios of NO, O_3 , H_2O (needed to calculate f) and the ozone photolysis rate were measured during MINATROC, while the OH, HO_2 and CH_3O_2 mixing ratios were calculated by the model (the run without isoprene is used here). The net ozone production rate is shown in Fig. 7a, and ranges between 0 and 7 ppbv/hr . During the major dust event relatively low ozone production rates are calculated. The daytime mean NOP is $0.33 \pm 0.24 \text{ ppbv/hr}$ during the major dust event and $1.06 \pm 1.37 \text{ ppbv/hr}$ in the dust-poor airmasses. The NOP is dominated by the primary production of O_3 , which can be seen as a good correlation between NOP and the NO mixing ratio in Fig. 7a. This also becomes clear in Fig. 7b, where the contribution of the different production and loss processes to the NOP is shown. The reactions of NO with HO_2 and CH_3O_2 dominate the net O_3 production rate. On the other hand, the loss terms are very small. The difference between dust-loaded and dust-poor airmasses is also determined by the difference in primary ozone production through the relatively low RO_x and NO mixing ratios in the Saharan airmasses.

Since the RO_x mixing ratio is overestimated by the box-model during the dust event, the NOP is also calculated using the measured RO_x values, maintaining the HO_2/RO_2 ratio as calculated by the boxmodel. Therefore, the modelled HO_2 and CH_3O_2 concentrations were scaled using the calc/obs ratio of RO_x . When doing so, the mean daytime NOP during the dust event decreased to $0.14 \pm 0.13 \text{ ppbv/hr}$, while the NOP in the dust-poor airmasses remained the same.

The relatively low RO_x and NO mixing ratios observed during the major dust event cause a significant reduction in the net ozone production rate, however, the values remain positive. On average the difference in daytime mean O_3 mixing ratio between the dust-loaded and dust-poor airmasses was 17 ppbv , while the difference in NOP was 0.73 and 0.92 ppbv/hr for the modelled and observed RO_x mixing ratios, respectively. Within 23 and 18 h of sunlight, respectively, a difference of 17 ppbv O_3 could be achieved, which corresponds to an air mass “age” of 2 to 3 days (assuming 10 h sunshine per day), which is close to the estimated age of the dust-loaded airmasses. However, since the ozone mixing ratios observed in the dust-loaded airmasses are relatively low, a net ozone production of $0.14\text{--}0.33 \text{ ppbv/hr}$ during the last three days would mean that the O_3 mixing ratio in the source region was even lower, about $25\text{--}30 \text{ ppbv}$. The low O_3 mixing ratio observed in the dust-loaded airmasses would then be attributed to the transport of O_3 poor air from the North African continent to the measurement site. On the other hand, the relatively high NO mixing ratios observed at the measurement site are at least partly due to transport from the local boundary layer, and probably not representative for the

NO mixing ratio during the last three days, which means that the airmass may have been subject to net ozone destruction during the first 2–2.5 days of its transport from the North African continent. Another possible cause for the low O₃ mixing ratios observed during the Saharan dust event is heterogeneous removal of O₃ on Saharan dust aerosol. Ozone destruction at the surface and cloud uptake could be important at this measurement site as well, however, it probably did not cause the difference between the O₃ mixing ratio observed in the dust-loaded and dust-poor air masses, since the cloud and surface conditions did not change during the campaign.

Due to the relatively high NO mixing ratios observed on several days during the MINATROC campaign, the average net ozone production rate is high compared to other campaigns. The daily average NOP ranged between 0.15 and 3.7 ppb_v/hr, and the corresponding daily average NO mixing ratio was between 27 and 265 ppt_v. During the first MINATROC campaign at Mt. Cimone the daytime mean NOP ranged between −0.1 and 0.3 ppb_v/hr for an average daily mean NO mixing ratio of about 40 ppt_v (Fischer et al., 2003), comparable to the days with lower NO mixing ratios at Izaña. At Mauna Loa, a mountain station at about the same latitude as Izaña, being much further away from pollution sources, net ozone destruction was found. During the summer of 1992 an average midday NOP of −0.15 ppb_v/hr was calculated at an average NO mixing ratio of 19 ppt_v (Cantrell et al., 1996).

7 Summary and conclusions

During the Saharan dust event reduced mixing ratios of O₃, RO_x, NO_x and H₂O₂ were observed compared to the rest of the campaign. The daytime mean O₃, NO_x and H₂O₂ mixing ratios dropped by 33%, 35% and 48% during the dust event, respectively, while the midday maximum RO_x mixing ratio decreased by 47% compared to the dust-poor days.

Using the MECCA chemistry box model, steady state concentrations of RO_x, HCHO and H₂O₂ were simulated and compared to the observed mixing ratios. The observed RO_x mixing ratios could be reproduced within a factor of two of the observed values, however, the variability of the modelled values was much lower than the variability in the observed mixing ratios. The calculated RO_x mixing ratio appeared to be rather insensitive to changes in the input concentrations of most trace gases, except for H₂O and O₃, which were constrained to the measured values in the model. Although the RO_x mixing ratios were overestimated during the major dust event, no clear relation to the presence of dust aerosol could be found.

The HCHO mixing ratio is significantly overestimated by the model, which could at least partly be explained by the neglect of dry deposition. The calculated HCHO mixing ratio is very sensitive to the input concentrations of isoprene and CH₃OOH, which are both subject to large measurement

uncertainties. It has been shown that the airmass might not have reached steady state with respect to isoprene (and other locally emitted biogenic species), and that a neglect of isoprene in the model simulations provides the best agreement with the measured HCHO and RO_x mixing ratios. Probably a combination of the neglect of dry deposition, an overestimation of the CH₃OOH and isoprene mixing ratios and the fact that the airmass might not be in steady state with respect to isoprene causes the disagreement between observation and boxmodel calculations. However, we cannot finally exclude the possibility of an underestimation of the observed HCHO mixing ratios.

The observed H₂O₂ mixing ratios could only be reproduced with the box model when dry deposition was included. However, even after including dry deposition, the H₂O₂ mixing ratios were strongly overestimated during the Saharan dust event. A much better agreement between the observed and calculated H₂O₂ mixing ratios could be achieved by adding heterogeneous removal reactions of HO₂ and H₂O₂. A relatively low H₂O₂ accommodation coefficient of 5×10^{-4} was sufficient to reproduce the observed H₂O₂ mixing ratios during the dust event. Good agreement between the model and observations was also obtained by considering heterogeneous removal of HO₂ with an accommodation coefficient of 0.2. However, if we assume that H₂O₂ is formed during the heterogeneous reaction of HO₂ on mineral dust aerosol, the additional H₂O₂ production had to be compensated with heterogeneous removal of H₂O₂ with a higher accommodation coefficient (2×10^{-3}) to obtain a good agreement between the modelled and observed values. Given that the measurements clearly indicate the uptake of HO₂ and/or H₂O₂ on Saharan dust aerosol, laboratory studies of the uptake of HO₂ and H₂O₂ on mineral dust aerosol are needed.

The low ozone mixing ratios observed during the Saharan dust event cannot be analysed with the boxmodel without making assumptions on the concentrations of O₃ and other trace gases in the dust source area. Therefore, we calculated the net ozone production rate for dust-loaded and dust-poor airmasses. Due to the relatively low RO_x and NO mixing ratios in the Saharan dust plume the NOP is significantly reduced compared to the dust-poor airmasses, which may explain the difference in O₃ mixing ratios observed in those airmasses. However, heterogeneous removal of O₃ on Saharan dust particles cannot be excluded. An average net ozone production rate of 0.14 ppb_v/hr has been calculated within the dust plume when the observed RO_x mixing ratios were used and 0.33 ppb_v/hr when the calculated RO_x mixing ratios were used. The daily average NOP ranged between 0.15 and 3.7 ppb_v/hr in the dust-poor airmasses, while the overall average daytime NOP was 1.06 ppb_v/hr.

Acknowledgements. We would like to thank E. Cuevas and his team for their technical support at the Izaña observatory and Astrid Kerkweg for her help with the modelling. The MINATROC project was financially supported by the European Commission (DG XII).

Edited by: W. T. Sturges

References

- Ayers, G. P., Gillet, R. W., Granek, H., de Serves, C., and Cox, R. A.: Formaldehyde production in clean marine air, *Geophys. Res. Lett.*, 24, 401–404, 1997.
- Bauer, S. E., Balkanski, Y., Schulz, M., and Haughlustaine, D. A.: Global modeling of heterogeneous chemistry on mineral aerosol surfaces: Influence on tropospheric ozone chemistry and comparison to observations, *J. Geophys. Res.*, 109, D02304, doi:10.1029/2003JD003868, 2004.
- Bian, H. and Zender, C. S.: Mineral dust and global tropospheric chemistry: Relative roles of photolysis and heterogeneous uptake, *J. Geophys. Res.*, 108, D21, 4672, doi:10.1029/2002JD003143, 2003.
- Bonasoni, P., Cristofanelli, P., Calzolari, F., Bonafe, U., Evangelisti, F., Stohl, A., Zauli Sajani, S., van Dingenen, R., Colombo, T., and Balkanski, Y.: Aerosol-ozone correlations during dust transport episodes, *Atmos. Chem. Phys.*, 4, 1201–1215, 2004, **SRef-ID: 1680-7324/acp/2004-4-1201**.
- Cantrell, C. A., Shetter, R. E., Gilpin, T. M., and Calvert, J. G.: Peroxy radicals measured during Mauna Loa Observatory Photochemistry Experiment 2: The data and first analyses, *J. Geophys. Res.*, 101, 14 643–14 652, 1996.
- Carslaw, N., Plane, J. M. C., and Coe, H.: Observations of the nitrate radical in the free troposphere at Izaña de Tenerife, *J. Geophys. Res.*, 102, 10 613–10 622, 1997.
- Clegg, S. M. and Abbatt, J. P. D.: Uptake of gas-phase SO₂ and H₂O₂ by ice surfaces: dependence on partial pressure, temperature and surface acidity, *J. Phys. Chem. A.*, 105, 6630–6636, 2001.
- Cooper, P. L. and Abbatt, J. P. D.: Heterogeneous interactions of OH and HO₂ radicals with surfaces characteristic of atmospheric particulate matter, *J. Phys. Chem.*, 100, 2249–2254, 1996.
- Crutzen, P. J. and Arnold, F.: Nitric-acid cloud formation in the cold Antarctic stratosphere – a major cause for the springtime ozone hole, *Nature*, 324, 651–655, 1986.
- Dentener, F. J., Carmichael, G. R., Zhang, Y., Lelieveld, J., and Crutzen, P. J.: Role of mineral aerosol as a reactive surface in the global troposphere, *J. Geophys. Res.*, 101, 22 869–22 889, 1996.
- de Reus, M., Dentener, F., Thomas, A., Borrmann, S., Ström, J., and Lelieveld, J.: Airborne observations of dust aerosol over the North Atlantic Ocean during ACE-2: indications for heterogeneous ozone destruction, *J. Geophys. Res.*, 105, 15 263–15 275, 2000.
- Fischer, H., Niktas, C., Parchatka, U., Zenker, T., Harris, G. W., Matuskas, P., Schmitt, R., Mihelcic, D., Muesgen, P., Paetz, H.W., Schultz, M., and Volz-Thomas, A.: Trace gas measurements during the Oxidizing Capacity of the Tropospheric Atmosphere campaign 1993 at Izana, *J. Geophys. Res.*, 103, 13 505–13 518, 1998.
- Fischer, H., Kormann, R., Klüpfel, T., Gurk, Ch., Königstedt, R., Parchatka, U., Mühle, J., Rhee, T. S., Brenninkmeijer, C. A. M., Bonasoni, P., and Stohl, A.: Ozone production and trace gas correlations during the June 2000 MINATROC intensive measurement campaign at Mt. Cimone, *Atmos. Chem. Phys.*, 3, 725–738, 2003, **SRef-ID: 1680-7324/acp/2003-3-725**.
- Fuchs, N. A. and Sutugin, A. G.: Highly Dispersed Aerosols, 105 pp., Butterworth-Heinemann, Woburn, Mass., 1970.
- Gros, V., Williams, J., van Aardenne, J. A., Salisbury, G., Hofmann, R., Lawrence, M. G., von Kuhlmann, R., Lelieveld, J., Krol, M., Berresheim, H., Lobert, J. M., and Atlas, E.: Origin of anthropogenic hydrocarbons and halocarbons measured in the summertime European outflow (on Crete in 2001), *Atmos. Chem. Phys.*, 3, 1223–1235, 2003, **SRef-ID: 1680-7324/acp/2003-3-1223**.
- Hanisch, F. and Crowley, J. N.: Ozone decomposition on Saharan dust: an experimental investigation, *Atmos. Chem. Phys.*, 3, 119–130, 2003, **SRef-ID: 1680-7324/acp/2003-3-119**.
- Hanke, M., Umann, B., Ueker, J., Arnold, F., and Bunz, H.: Atmospheric measurements of gas-phase HNO₃ and SO₂ using chemical ionization mass spectrometry during the MINATROC field campaign 2000 on Mont Cimone, *Atmos. Chem. Phys.*, 3, 417–436, 2003, **SRef-ID: 1680-7324/acp/2003-3-417**.
- Hanson, D. R., Burkholder, J. B., Howard C. J., and Ravishankara, A. R.: Measurement of OH and HO₂ radical uptake coefficients on water and sulphuric acid surfaces, *J. Phys. Chem.*, 96, 4979–4985, 1992.
- Heikes, B. G. and Thompson, A. M.: Effects of heterogeneous processes on NO₃, HONO and HNO₃ chemistry in the troposphere, *J. Geophys. Res.*, 88, 10 883–10 895, 1983.
- Heikes, B., Lee, M., Jacob, D., Talbot, R., Bradshaw, J., Singh, H., Blake, D., Anderson, B., Fuelberg, H., and Thompson, A. M.: Ozone, hydroperoxides, oxides of nitrogen, and hydrocarbon budgets in the marine boundary layer over the South Atlantic, *J. Geophys. Res.*, 101, 24 221–24 234, 1996.
- IPCC (Intergovernmental Panel on Climate Change): Climate change 1995, edited by: Houghton, J. T., Meira Filho, L. G., Callender, B. A., Harris, N., Kattenberg, A., and Maskell, A., Cambridge University Press, Cambridge, UK, 572 p., 1996.
- Jacob, D. J.: Heterogeneous chemistry and tropospheric ozone, *Atm. Environ.*, 34, 2131–2159, 2000.
- Jaeglé, L., Jacob, D. J., Brune, W. H., Faloon, I., Tan, D., Heikes, B. G., Kondo, Y., Sachse, G. W., Anderson, B., Gregory, G. L., Singh, H. B., Poeschel, R., Ferry, G., Blake, D. R., and Shetter, R. E.: Photochemistry of Hox in the upper troposphere at northern latitudes, *J. Geophys. Res.*, 105, 3877–3892, 2000.
- Junkermann, W. and Stockwell, W. R.: On the budget of photooxidants in the marine boundary layer of the tropical South Atlantic, *J. Geophys. Res.*, 104, 8039–8046, 1999.
- Kormann, R., Fischer, H., de Reus, M., Lawrence, M., Bruhl, C., von Kuhlmann, R., Holzinger, R., Williams, J., Lelieveld, J., Warneke, C., de Gouw, J., Heland, J., Ziereis, H., and Schlager, H.: Formaldehyde over the eastern Mediterranean during MINOS: Comparison of airborne in-situ measurements with 3D-model results, *Atmos. Chem. Phys.*, 3, 851–861, 2003, **SRef-ID: 1680-7324/acp/2003-3-851**.
- Lazrus, A. L., Kok, G. L., Lind, J. A., Gitlin, S. N., Heikes, B. G., and Shetter, R. E.: Automated fluorometric method for hydrogen-peroxide in air, *Anal. Chem.*, 58, 594–597, 1986.
- Lelieveld, J. and Crutzen, P. J.: Influences of cloud photochemical processes on tropospheric ozone, *Nature*, 343, 227–233, 1990.
- Lelieveld, J., van Aardenne, J., Fischer, H., de Reus, M., Williams, J., and Winkler, P.: Increasing ozone over the Atlantic Ocean, doi:10.1126/science.1096777, *Science*, 2004.

- Lindinger, W., Hansel, A., and Jordan, A.: On-line monitoring of volatile organic compounds at pptv levels by means of Proton-Transfer-Reaction Mass Spectrometry (PTR-MS): Medical applications, food control and environmental research, *Int. J. Mass Spectrom. Ion Processes*, 173, 191–241, 1998.
- Liu, S. C., Kley, D., McFarland, M., Mahlmann, J. D., and Levi, H.: On the origin of tropospheric ozone, *J. Geophys. Res.*, 85, 7546–7552, 1980.
- Madronich, S., and Flocke, S.: The role of solar radiation in atmospheric chemistry, in: *Handbook of Environmental Chemistry*, edited by: Boule, P., Springer-Verlag, Heidelberg, pp. 1–26, 1998.
- Mozurkewich, M., McMurry, P. H., Gupta, A., and Calvert, J. G.: Mass accommodation coefficient for HO₂ radicals on aqueous particles, *J. Geophys. Res.*, 92, 4163–4170, 1987.
- Novelli, P. C., Masarie, K. A., Lang, P. M., Hall, B. D., Myers, R. C., and Elkins, J. W.: Reanalysis of tropospheric CO trends: Effects of the 1997–1998 wildfires, *J. Geophys. Res.*, 108, D15, 4464, doi:10.1029/2002JD003031, 2003.
- Olson, J. R., Crawford, J. H., Chen, G., Fried, A., Evans, M. J., Jordan, C. E., Sandholm, S. T., Davis, D. D., Anderson, B. E., Avery, M. A., Barrick, J. D., Blake, D. R., Brune, W. H., Eisele, F. L., Flocke, F., Harder, H., Jacob, D. J., Kondo, Y., Lefer, B. L., Martinez, M., Mauldin, R. L., Sachse, G. W., Shetter, R. E., Singh, H. B., Talbot, R. W., and Tan, D.: Testing fast photochemical theory during TRACE-P based on measurements of OH, HO₂ and CH₂O, *J. Geophys. Res.*, 109, D15S10, doi:10.1029/2003JD004278, 2004.
- O' Sullivan, D. W., Heikes, B. G., Lee, M., Chang, W., Gregory, G. L., Blake, D. R., and Sachse, G. W.: Distribution of hydrogen peroxide and methylhydroperoxide over the Pacific and South Atlantic Oceans, *J. Geophys. Res.*, 104, 5635–5646, 1999.
- Salisbury, G., Williams, J., Holzinger, R., Gros, V., Mihalopoulos, N., Vrekousis, M., Sarda-Esteve, R., Berresheim, H., von Kuhlmann, R., Lawrence, M., and Lelieveld, J.: Ground-based PTR-MS measurements of reactive organic compounds during the MINOS campaign in Crete, July–August 2001, *Atmos. Chem. Phys.*, 3, 925–940, 2003,
SRef-ID: 1680-7324/acp/2003-3-925.
- Sander, R., Kerkweg, A., Jöckel, P., and Lelieveld, J.: Technical Note: The new comprehensive atmospheric chemistry module MECCA, *Atmos. Chem. Phys. Discuss.*, 4, 7167–7180, 2004,
SRef-ID: 1680-7375/acpd/2004-4-7167.
- Sander, S. P., Finlayson-Pitts, B. J., Friedl, R. R., Golden, D. M., Huie, R. E., Kolb, C. E., Kurylo, M. J., Molina, M. J., Moortgat, G. K., Orkin, V. L., and Ravishankara, A. R.: Chemical Kinetics and photochemical data for use in atmospheric studies, Evaluation number 14, JPL Publications 02-25, Jet Propulsion Laboratory, Pasadena, CA, 2003.
- Schultz, M.: Die Bedeutung von Stickoxiden für die Ozonbilanz in Reinluftgebieten, Untersuchung der Photochemie in Reinluft anhand von Spurengasmessungen auf Teneriffa, Ph.D. thesis, Bergischen Universität Wuppertal, Germany, 185 p., 1995.
- Singh, H. B., Salas, L. J., Chatfield, R. B., Czech, E., Fried, A., Walega, J., Evans, M., Field, B. D., Jacob, D. J., Blake, D., Heikes, B., Talbot, R., Sachse, G., Crawford, J. H., Avery, M. A., Sandholm, S., and Fuelberg, H.: Analysis of the atmospheric distribution, sources, and sinks of oxygenated volatile organic chemicals based on measurements over the Pacific during TRACE-P, *J. Geophys. Res.*, 109, D15S07, doi:10.1029/2003JD003883, 2004.
- Tang, Y., Carmichael, G. R., Kurata, G., Uno, I., Weber, R. J., Song, C. H., Guttikunda, S. K., Woo, J. H., Streets, D. G., Wei, C., Clarke, A. D., Huebert, B., and Anderson, T. L.: Impacts of dust on regional tropospheric chemistry during the ACE-Asia experiment: A model study with observations, *J. Geophys. Res.*, 109, D19S21, doi:10.1029/2003JD003806, 2004.
- Underwood, G. M., Li, P., Al-Abadleh, H., and Grassian, V. H.: A Knudsen cell study of the heterogeneous reactivity of nitric acid on oxide and mineral dust particles, *J. Phys. Chem. A*, 105, 6609–6620, 2001.
- Usher, C. R., Michel, A. E., and Grassian, V. H.: Reactions on mineral dust, *Chem. Rev.*, 103, 4883–4939, 2003.
- von Kuhlmann, R., Lawrence, M. G., Crutzen, P. J., and Rasch, P. J.: A model for studies of tropospheric ozone and non-methane hydrocarbons: Model description and ozone results, *J. Geophys. Res.*, 108, D9, doi:10.1029/2002JD002893, 2003.
- Wagner, V., von Glasow, R., Fischer, H., and Crutzen, P. J.: Are CH₂O measurements in the marine boundary layer suitable for testing the current understanding of CH₄ photooxidation?: A model study, *J. Geophys. Res.*, 107, D3, doi:10.1029/2001JD000722, 2002.
- Weinstein-Lloyd, J. B., Lee, J. H., Daum, P. H., Kleinman, L. I., Nunnermacker, L. J., Springston, S. R., and Newman, L.: Measurements of peroxides and related species during the 1995 summer intensive of the Southern Oxidants Study in Nashville, Tennessee, *J. Geophys. Res.*, 103, 22 361–22 373, 1998.
- Weller, R., Schrems, O., Boddenberg, A., Gäb, S., and Gautrois, M.: Meridional distribution of hydroperoxides and formaldehyde in the marine boundary layer of the Atlantic (48°N–35°S) measured during the Albatross campaign, *J. Geophys. Res.*, 105, 14 401–14 412, 2000.
- Williams, J., Pöschl, U., Crutzen, P. J., Hansel, A., Holzinger, R., Warneke, C., Lindinger, W., and Lelieveld, J.: An atmospheric chemistry interpretation of mass scans obtained from a proton transfer mass spectrometer flown over the tropical rainforest of Surinam, *J. Atmos. Chem.*, 38, 133–166, 2001.
- Worsnop, D. R., Zahniser, M. S., Kolb, C. E., Gardner, J. A., Watson, L. R., Van Doren, J. M., Jayne, J. T., and Davidovits, P.: Temperature dependence of mass accommodation of SO₂ and H₂O₂ on aqueous surfaces, *J. Phys. Chem.*, 93, 1159–1172, 1989.
- Zaveri, R. A., Saylor, R. D., Peters, L. K., McNider, R., and Song, A.: A model investigation of summertime diurnal ozone behaviour in rural mountainous locations, *Atmos. Environ.*, 29, 1043–1065, 1995.
- Zhang, Y., Sunwoo, Y., Kotamarthi, V., and Carmichael, G. R.: Photochemical oxidant processes in the presence of dust: an evaluation of the impact of dust on particulate nitrate and ozone formation, *J. Appl. Meteorol.*, 33, 813–824, 1994.
- Zhang, Y. and Carmichael, G. R.: The role of mineral aerosol in tropospheric chemistry in East Asia – a model study, *J. Appl. Meteorol.*, 38, 353–366, 1999.
- Zhou, X., Lee, Y. N., Newman, L., Chen, X., and Mopper, K.: Tropospheric formaldehyde concentrations at the Mauna Loa Observatory during the Mauna Loa Observatory Photochemistry Experiment 2, *J. Geophys. Res.*, 101, 14 711–14 719, 1996.